

Ultrafast multireflector physical-optics beam simulations for the HFI instrument on the ESA PLANCK Surveyor

Vladimir B. Yurchenko^a, John Anthony Murphy^a and Jean-Michel Lamarre^b

^aExperimental Physics Dept., National University of Ireland, Maynooth, Co. Kildare, Ireland;

^bObservatoire de Paris, 61 Av de l'Observatoire, 75014, Paris, France

ABSTRACT

We present the latest results of our fast physical optics simulations of the ESA PLANCK HFI beams. The main beams of both polarized and non-polarized channels have been computed with account of broad frequency bands for the final design and positions of the HFI horns. Gaussian fitting parameters of the broadband beams have been presented. Beam polarization characteristics and horn defocusing effects have been studied.

Keywords: ESA PLANCK, HFI, CMB, Polarization, Physical Optics

1. INTRODUCTION

With increasing the size and complexity of the space-based antennas for radioastronomy, there is a demand for increasing the efficiency of simulations of large multi-reflector telescope systems. A typical example is the ESA PLANCK Surveyor, the 3rd generation deep-space submillimeter-wave telescope being designed for measuring the temperature anisotropies and polarization of the Cosmic Microwave Background (CMB). The telescope will be equipped with two focal plane instruments, the Low-Frequency and High-Frequency Instruments, for detecting the radiation in the frequency range from 30 GHz to 1000 GHz in nine bands.¹

The High-Frequency Instrument (HFI) will operate in six frequency channels² centered at 100, 143, 217, 353, 545 and 857 GHz. Four channels (100 – 353 GHz) will use mono-mode quasi-Gaussian horns,³ half of them feeding polarization sensitive bolometers⁴ (PSB). The other two channels (545 and 857 GHz) are feeding non-polarized bolometers and use profiled multi-mode horns. All the HFI horns are broadband, with the bandwidth being about 30% of central frequency. The system is designed to meet the extreme requirements on both the primary mirror edge taper (–25 dB) and the angular resolution on the sky (about 5 arcminutes at the frequencies of 217 – 857 GHz).

Due to the off-axis horn positions and the dual-mirror design of telescope, the beam shapes on the sky are far from circular (see Table 2). Their exact representation requires mapping with a significant number of points. This becomes important because the simulation and data reduction of the Planck mission will be huge tasks requiring enormous computing power. A first step towards feasibility of computations is to model the beams by analytical functions that can be handled more efficiently than the raw data.⁵

The aim of this paper is to present the results of the PLANCK HFI beam computations and to provide the update to the earlier published beam data⁶ that can be used as a reference for simulations of the Planck mission and for the development of its data processing tools.

2. SIMULATIONS OF THE MAIN BEAMS

Simulations of the PLANCK HFI beams are extremely challenging because of asymmetric dual-reflector geometry of the telescope, large primary mirror having projected diameter $D = 1.5$ m ($D/\lambda_{min} = 5000$), a very wide field of view, broadband and multi-mode structure of the horn fields, and strict requirements on the accuracy. Physical optics (PO) is the most adequate technique for this kind of computations. Conventional software, however, cannot cope efficiently with problems of this size in full PO+PO mode of simulations.

Send correspondence to: v.yurchenko@may.ie; phone: +353 1 708 3746; fax: +353 1 708 3313

As an alternative, we developed a dedicated fast PO simulation method which is specifically designed for large multi-beam multi-reflector systems with broadband channels and multi-mode structure of the horn field.^{7,8} The method allows us to perform rigorous PO+PO TE/TM-mode simulations of the main beams of large telescopes such as PLANCK in a few minutes for mono-mode mono-frequency channels (as the beams transmitted by telescope) and in about an hour for the broad-band polarization-averaged multi-mode channels of the highest frequencies.

We compute the beam patterns of the *IQUV* Stokes parameters on the sky by propagating the source field from the apertures of corrugated horns through the telescope mode-by-mode, with integration over the frequency band and with account of all polarizations of the field of non-polarized channels.⁸ The aperture field of horns has been computed by the scattering matrix approach.⁹ The effective modes of the electric field at the horn aperture, E_{nm} , are represented via the canonical TE-TM modes $\vec{\mathcal{E}}_{nj}$ of a cylindrical waveguide as follows

$$\vec{E}_{nm}(\rho, \varphi) = \sum_{j=1, \dots, 2M} S_{nmj} \vec{\mathcal{E}}_{nj}(\rho, \varphi) \quad (1)$$

where $S_{nmj} = S_{nmj}(f)$ is the scattering matrix provided by E. Gleeson⁹ for each horn at various frequencies f (S_{nmj} is used as an input in this work), $n = 0, 1, \dots, N$ is the azimuthal index and $m, j = 1, 2, \dots, 2M$ are the radial indices accounting for both the TE ($m, j = 1, \dots, M$) and TM ($m, j = M + 1, \dots, 2M$) modes.

The beam data are computed assuming smooth telescope mirrors of ideal elliptical shape, of perfect electrical conductivity of their reflective surfaces, and of ideal positioning of mirrors and horn antennas. The total beam power is found as a sum of powers of all modes propagated to the sky with account of all contributing polarization directions. Similarly, the broadband beam patterns of Stokes parameter are the sums of the relevant patterns of all the modes at all the frequencies of the bandwidth. In mono-mode beams, the E_{nm} modes sum up effectively to a single mode which is of one unit of total power, almost Gaussian in shape and, for the polarized channels, of nearly perfect linear polarization on the horn aperture.

Our latest simulations of the PLANCK HFI beams provide the updates to the beam data published in Ref. 6. There are five essential corrections to those data: (1) the horn design is slightly changed (mainly, due to the manufacturing procedure) so that the horns are slightly elongated compared to those in Ref. 6, (2) the horn positions are now the final ones, (3) both broadband and monochromatic beams are computed, (4) root-mean-square beam fitting is performed, (5) the gains of mono-mode non-polarized beams are corrected (they should be increased in Ref. 6 by 3 dB while the gains of multi-mode horns remain correct for those horns at those positions).

The horn positions are specified by the aperture refocus parameter $R_A = R_F + R_C$ where R_A is the distance along the horn axis from the reference detector plane to the horn aperture, R_F is the similar distance to the point F of the geometrical focus of telescope on this axis, and R_C is the distance from the point F to the horn aperture. The best refocus R_{A0} is found by minimizing the angular width of the broad-band beams (simultaneously, it appears to maximize the gain, even in the case of complicated multi-mode beams). At the best refocus, $R_{C0} = R_{A0} - R_F$ specifies the focal center of the horn. This is the point inside the horn which is superimposed with the telescope focal point F when $R_A = R_{A0}$.

The horn positions used in this paper are those of the final design. They differ in some cases from the ones used in Ref. 6. The final positions are specified by the values of R_C in Table 1. Generally, these R_C are sufficiently close to the best refocus values R_{C0} found for the broadband horns of the final design (Fig. 1).

Table 1. Position parameter R_C used in simulations (p or n means polarized or non-polarized horns)

HFI beam	100-1,4	100-2,3	143-p	143-n	217-p	217-n	353-p	353-n	545-n	857-n
R_C , mm	1.2	1.4	1.2	3.5	1.1	1.3	1.5	1.5	4.0	4.0

Measuring polarization with bolometric detectors requires comparisons of signals of four polarization channels obtained from the same pixel on the sky. To minimize polarization errors due to mismatch of different

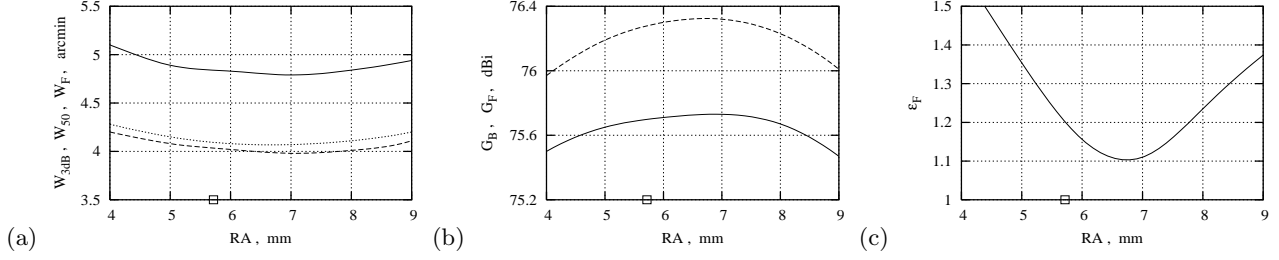


Figure 1. HFI-545-4 horn defocusing effects: broadband beam (a) width W_{3dB} , W_{50} and W_F (solid, dashed and dotted curve, respectively), (b) gain G_B and G_F (solid and dashed curve, respectively), and (c) ellipticity ϵ_F (see Section 4) as a function of the horn aperture refocus parameter R_A (point shows the design value of R_A when $R_C = 4.0$ mm).

beams, pairs of orthogonal polarization channels (a, b) are built into each horn by using polarization-sensitive bolometers.⁴ The two other measurements needed to evaluate the Q and U Stokes parameters are obtained less than a second later, when the sister beam observes the same pixel, due to the spinning of the satellite.

Broad frequency bands improve the power and polarization patterns of the HFI beams compared to those in Refs. 6: the difference of the broadband I patterns of two channels of the same beam is less than 1% of maximum power (Fig. 2, a). The mismatch of sister beams when superimposed on the sky is much greater (up to 5 – 8%) and depends on the horn location in the focal plane.^{6, 8} The difference of the mono-frequency and broadband I patterns of the same beam normalized to the unit total power is, typically, about 1 – 2% (Fig. 2, b).

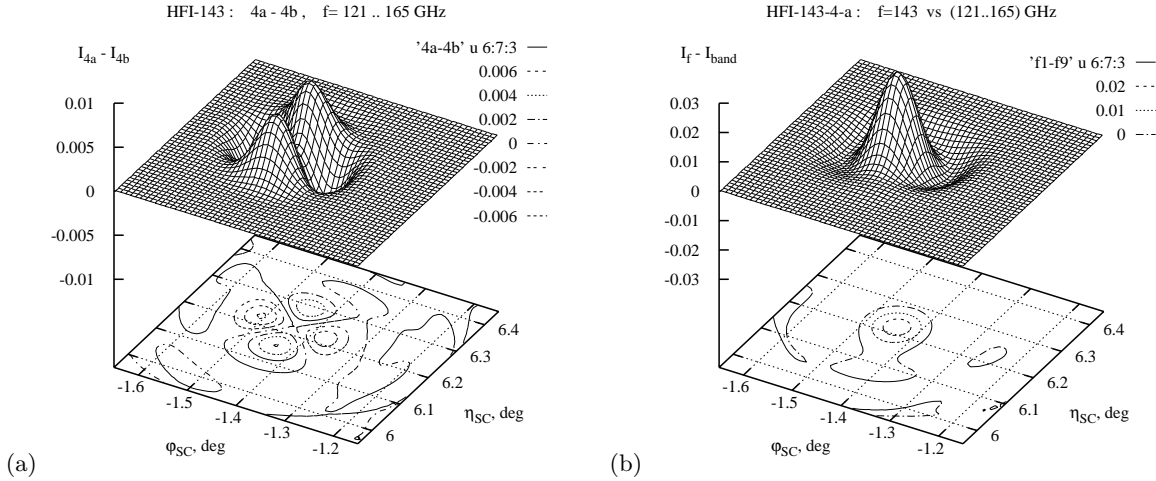


Figure 2. The difference of the broadband intensity patterns of (a) two channels of orthogonal polarization of the same beam HFI-143-4-a/b and (b) mono-frequency and broadband beam HFI-143-4a.

3. GAUSSIAN FITTING OF THE PLANCK HFI BEAMS

As a development of previous work,⁶ in this paper we compute the broadband HFI beams (Fig. 3). The broadband computations are particularly important for the multi-mode beams which have a complicated modal structure depending essentially on the frequency within the band. These beams are computed using up to 11 modes in the band $f = 455 - 635$ GHz for the HFI-545 beams and up to 16 modes in the band $f = 716 - 998$ GHz for the HFI-857 beams. All the HFI beams are computed with nine sampling frequencies in each frequency band that is sufficient for the broadband simulations in the limited area of the main beams. The main results including the Gaussian fitting parameters of the beams are presented in Table 2.

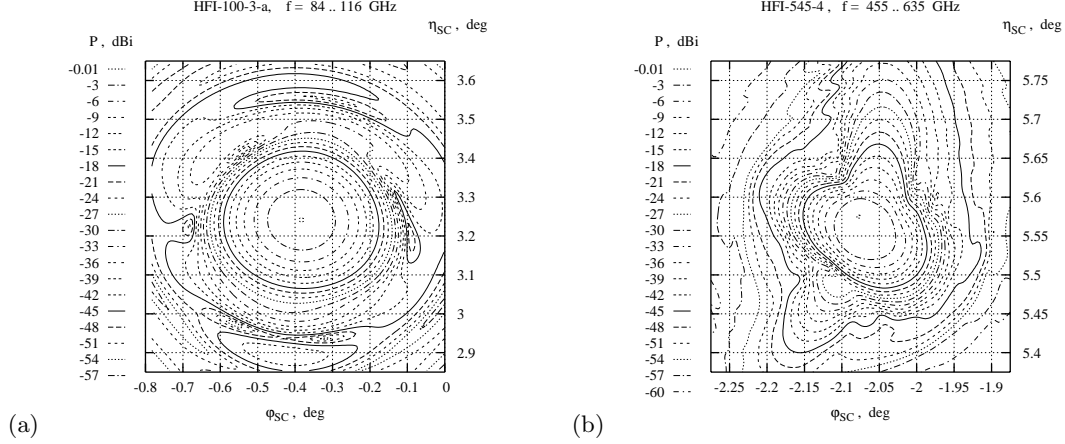


Figure 3. Broadband power patterns of (a) HFI-100-3a and (b) HFI-545-4 beams computed for the final design and positions of horns (cf respective mono-frequency patterns in Ref. 6).

The *IQUV* beam patterns are presented as functions of the $(\varphi_{SC}, \eta_{SC})$ coordinates on the sky ($\eta_{SC} = 90^\circ - \theta_{SC}$) as viewed from the sky to the telescope in the spherical frame of spacecraft (SC), with the azimuthal and polar angles φ_{SC} and θ_{SC} , respectively, and with the polar axis being the nominal spin axis of telescope (the center of the focal plane corresponds to $\varphi_{SC} = 0^\circ$ and $\eta_{SC} = 5^\circ$). In this representation, the Q and U Stokes parameters, being frame-dependent, are defined with respect to φ_{SC} as the first axis (pointing to the right when viewed from the sky to the telescope) and η_{SC} as the second axis (pointing upwards).

The polarization angle Ψ_E of the beam field is measured from the positive direction of the φ_{SC} axis to the direction of major axis of polarization ellipse of the electric field \vec{E} , with the positive angles counted towards the positive direction of the η_{SC} axis. So, Ψ_E is measured counter-clockwise from the parallels of the SC frame as viewed from the sky, in accordance with the definition of Q and U . In this case, $\tan(2\Psi_E) = U/Q$. This equation allows one to compute the polarization angle of the polarized component of partially polarized incoherent beams using the broadband values of U and Q .

The nominal values of Ψ_E for the a-channels are $\Psi_E = 135^\circ$ for the beams HFI-143-1/2, 217-5/6 and 353-3/4, $\Psi_E = 90^\circ$ for the beams HFI-143-3/4, 217-7/8 and 353-5/6, and $\Psi_E = 112.5^\circ, 135^\circ, 90^\circ$ and 67.5° for the beams HFI-100-1, 2, 3 and 4, respectively. The complementary b-channels have the PSB polarization directions in the horns precisely orthogonal to those of a-channels. On the sky, non-orthogonality of polarization is less than 0.03° for the beam-average angles Ψ_E and, typically, less than 0.10° for the polarization angles on the beam axes. Generally, the beam-average angles Ψ_E coincide with the required nominal values better than by 0.01° , though some on-axis values may differ by about 0.1° .

For the polarized beams, along with the distortion of polarization, some depolarization appears when the field propagates from the ideal PSB through the horn and the telescope. Similarly, for the non-polarized beams, small polarization arises. These effects are represented by the deviations of the *QUV* Stokes parameters from the ideal values across the beam patterns. The bounds on these non-idealities are found as $\delta V = \max(|V|/I_{max})$ and $\delta L = \max(\delta Q, \delta U)$ where $\delta Q = \max(|Q - Q_0|/I_{max})$, $\delta U = \max(|U - U_0|/I_{max})$ and $I_{max} = \max(I)$, with Q_0 and U_0 being the ideal values of Q and U , respectively (the values when the degree of polarization is either one or zero and the polarization angle Ψ_E is equal to its nominal value across the whole beam). Notice, that the beam-average non-idealities δV_B and δL_B are much smaller than the maximum values δV and δL .

In this work, we fit the intensity Stokes parameter patterns $I(\varphi_{SC}, \eta_{SC})$ by the elliptical Gaussian beams $F(\varphi_{SC}, \eta_{SC})$. We normalize all the Stokes parameters so that $\max(I) = 1$. In the original PO simulated beams, the power per one steradian, P [Watt/sr], is computed with account of all contributing modes and polarizations, in the units of power P_0 [Watt/sr] radiated per one steradian by an isotropic source with the power of one mode of single polarization. Then, the original patterns $P(\varphi_{SC}, \eta_{SC})$, when presented in dBi, are computed as follows

$$P(\varphi_{SC}, \eta_{SC})[\text{dBi}] = 10\log_{10}\{I(\varphi_{SC}, \eta_{SC})\} + P_{max}[\text{dBi}] \quad (2)$$

where P_{max} [dBi] is the power gain of the original beam in the units of power P_0 of an isotropic source of one mode of single polarization. The power of one mode constituting the unit P_0 is defined as being radiated (or received) by the bolometer of the given cross-section s_B accounted in the scattering matrix S_{nmj} .

With the incident radiation characterized by the Stokes parameters $\{I_{sky}, Q_{sky}, U_{sky}, V_{sky}\}$ (in absolute units, so that $I_{sky}[\text{Watt}/(\text{sr} \cdot \text{Hz})]$ is the sky brightness), the total power S_α [Watt] absorbed by the bolometer in the frequency band Δf (the channel response) is evaluated as

$$S_\alpha = 0.5P_{max} \int df \int d\Omega \{II_{sky} + QQ_{sky} + UU_{sky} + VV_{sky}\} \quad (3)$$

where P_{max} [rel.un.] is related to the beam gain P_{max} [dBi] in Eq. (2) as $P_{max}[\text{dBi}] = 10\log_{10}\{P_{max}[\text{rel.un.}]\}$ and $d\Omega$ is the element of solid angle (the gains in Table 2 are given per unit frequency range).

For the beam fitting, we use the elliptical Gaussian function

$$F(\varphi_{SC}, \eta_{SC}) = A \exp[-(p^2/a^2 + t^2/b^2)], \quad (4)$$

where $p = x\cos(\tau) + y\sin(\tau)$, $t = -x\sin(\tau) + y\cos(\tau)$, $x = \varphi_{SC} - \varphi_{SC0}$, $y = \eta_{SC} - \eta_{SC0}$, $a = 0.5W_{max}/q$, $b = 0.5W_{min}/q$, $q = \sqrt{\ln(2)}$, φ_{SC0} and η_{SC0} are the angular coordinates of the center point (the point of maximum power) of the fitting elliptical Gaussian beam in the SC frame, W_{max} and W_{min} are the full beam widths at half magnitude measured along the major and minor axes of the fitting beam ellipse, respectively, and τ is the angle from the φ_{SC} axis to the major axis of the beam ellipse measured counter-clockwise as viewed from the sky to the telescope (Fig. 4, a).

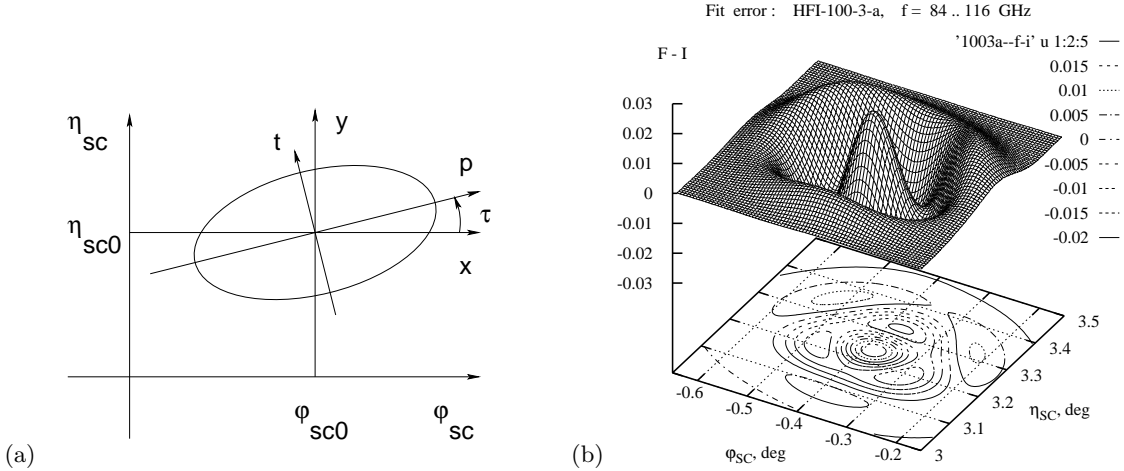


Figure 4. (a) Parameters of the elliptical fitting beam and (b) fitting error of the broadband beam HFI-1003-a (cf Ref. 6).

According to this definition, for each HFI beam, there are six fitting parameters (W_{max} , W_{min} , φ_{SC0} , η_{SC0} , τ , and A) which can be found by minimizing the relevant aim function that quantifies the deviation of the elliptical Gaussian fit from the given PO simulated beam. One can propose a variety of the aim functions to evaluate the difference between the fit and the actual beam. Because the basic quantity of interest is the power contribution to the PSB readout, it is the deviation of the beam power profile from the Gaussian fit that has to be minimized. Still, even in this special case, the aim function can be defined in various ways, see Ref. 6.

Unlike the options listed in Ref. 6, in this paper we use the root-mean-square (RMS) misfit of the beam pattern as the aim function. The latter is defined as

$$\Delta F = \left(\int (F - I)^2 d\Omega \right)^{1/2} / \int I d\Omega, \quad (5)$$

though the fitting error in Table 2 is estimated as the maximum of $\delta F = |F - I|$. In addition, we require the conservation of the total power of the beam $P_B = \int F d\Omega = \int I d\Omega$ so that the number of independent fitting parameters reduces to five.

4. RESULTS AND COMMENTS

The RMS Gaussian fitting parameters of the broadband HFI beams are shown in Table 2. Table 2 shows also some other parameters of the HFI beams such as the full width at the 3dB level of the original PO simulated beam ($W_B = W_{3dB}$), the mean full width at half magnitude of the Gaussian fitting beam $W_F = (W_{max}W_{min})^{1/2}$, the original beam gain $G_B[\text{dBi}] = P_{max}[\text{dBi}]$, the fitting beam gain $G_F[\text{dBi}] = P_{max}[\text{dBi}] + 10\log_{10}(A)$, the fitting beam ellipticity $\epsilon_F = W_{max}/W_{min}$, the maximum fit error δF , and the bounds δL and δV on the peak deviations of the QUV Stokes parameters of the original beams from the ideal values.

Overview of the data in Table 2 shows that the peak errors of the elliptical Gaussian fit with respect to the original beams is, typically, about 2% of maximum power for the mono-mode quasi-Gaussian beams HFI-100, 143, 217 and 353 (Fig. 4, b), while being up to 40% for the essentially flat-top multi-mode beams HFI-545 and 857. The error of 2% is quite significant, being comparable to the difference between mono-frequency and broad-band beams of polarized channels and usually greater than the difference between the beams of orthogonal polarizations of the same horns (see Section 2). This means that the elliptical Gaussian fit should be considered as a first term of a more advanced fitting to be developed later.

On the other hand, the fitting error remains smaller than the typical difference between the beams of two different complementary horns (the latter is about 5%). It means that the elliptical Gaussian fits are quite capable of accounting for the beam mismatch effects essential for polarization measurements.

Another essential observation is that the beam width of the Gaussian fit, W_F , is noticeably smaller than the typical width of the original beam, W_B , evaluated as a diameter of the circle of the same area as bounded by the 3dB isolevel ($W_B = W_{3dB}$), though it is close to the diameter of the area bounded by the isolevel encompassing 50% of the total power of the beam ($W_B = W_{50}$), see Fig. 1, a. The reason is that the real beams have specific shape at the top, tending to be flat-top, though more complicated. This happens even to quasi-Gaussian beams (more so to the broadband ones, see Fig. 2, b) both due to the field propagation via the horns and via the telescope, though multi-mode beams are significantly more flat-top because of their complicated modal composition. As a result, the original beams at half magnitude are always wider compared to the Gaussian fits at their half magnitude, respectively. More complicated beam fitting, when using additional terms, would be able to represent the width of the original beams with a better accuracy.

5. CONCLUSION

We present the results of our simulations of the broadband HFI beams of the ESA PLANCK Surveyor. The beams are computed by multi-mode physical optics propagation of the source field from the apertures of corrugated horns simulated by the scattering matrix approach. The horns of the final design at the actual positions in the focal plane of the telescope have been used.

Broad frequency bands of the HFI channels are shown to improve both the beam power and polarization patterns. Perfect alignment of polarization along the required directions is confirmed by small and symmetric deviations of the respective Q or U patterns from the ideal values. Peak difference of power patterns of orthogonal polarization channels, due to the usage of orthogonal pairs of polarization sensitive bolometers in the individual horns, is less than 1%, while it is 5% to 8% for the different beams of complementary pairs of horns designed for the polarization measurements.

Compact representations of the $IQUV$ patterns by a few parameters of the elliptical Gaussian fitting function are found. This approximation is generally considered as acceptable from the scientific viewpoint, although we show that induced errors are far from negligible.

New simulation technique proves indispensable for multi-reflector systems with a very wide field of view, large number of beams and complicated structure of propagating waves, when efficient and rigorous simulations of the main beams are needed.

ACKNOWLEDGMENTS

This work was supported in part by the Enterprise Ireland Basic Research Grant and the French-Irish Ulysses Research Visit Grants 2002 and 2003.

The authors are grateful to B. Maffei for the horn design, to E. Gleeson for the scattering matrix coefficients of the horn fields, and to Y. Longval for providing the positions of the telescope focal points and orientations of the horn axes.

REFERENCES

1. J. A. Tauber, “The PLANCK Mission: Overview and Current Status,” *Astrophys. Lett. Comm.* **37**, pp. 145–150, 2000.
2. J.-M. Lamarre et al., “The Planck High Frequency Instrument, a Third Generation CMB Experiment, and a Full Sky Submillimeter Survey,” *New Astronomy Reviews* **47**, pp. 1017–1024, 2003.
3. B. Maffei, P. A. R. Ade, C. E. Tucker, E. Wakui, R. J. Wylde, J. A. Murphy, and R. M. Colgan, “Shaped Corrugated Horns for Cosmic Microwave Background Anisotropy Measurements,” *Int. J. Infrared and Millimeter Waves* **21**, pp. 2023–2033, 2000.
4. A. D. Turner et al., “Silicon Nitride Micromesh Bolometer Array for Submillimeter Astrophysics,” *Applied Optics* **40**, pp. 4921–4932, 2001.
5. P. Fosalba, O. Dore, and F. R. Bouchet, “Elliptical Beams in CMB Temperature and Polarization Anisotropy Experiments: An Analytic Approach,” *Phys. Rev. D* **65** 063003-16, 2002.
6. V. B. Yurchenko, J. A. Murphy, J.-M. Lamarre, and J. Brossard, “Gaussian Fitting Parameters of the ESA PLANCK HFI Beams,” *Int. J. Infrared and Millimeter Waves* **25**, pp. 601–616, 2004.
7. V. B. Yurchenko, J. A. Murphy, and J.-M. Lamarre, “Fast Physical Optics Simulations of the Multi-Beam Dual-Reflector Submillimeter-Wave Telescope on the ESA PLANCK Surveyor,” *Int. J. Infrared and Millimeter Waves* **22**, pp. 173–184, 2001.
8. V. B. Yurchenko, J. A. Murphy, and J.-M. Lamarre, “Simulation and Comparison of the PLANCK HFI Beams with Implications on Polarization Measurements,” in *3rd ESA Workshop on Millimeter Wave Technology and Applications*, J. Mallat, A. Raisanen, and J. Tuovinen, eds., pp. 187–192, Millilab, Espoo, Finland, May 21–23, 2003.
9. E. Gleeson, J. A. Murphy, B. Maffei, J.-M. Lamarre, and R. J. Wylde, “Definition of the Multi-Mode Horns for the HFI Instrument on PLANCK,” in *25th ESA Antenna Workshop on Satellite Antenna Technology*, K. van ’t Klooster and L. Fanchi, eds., pp. 649–655, ESTEC, Noordwijk, The Netherlands, Sept. 18–20, 2002.

Table 2. Gaussian fitting parameters and some representative characteristics of the *broadband* PLANCK HFI beams (horns are located at the final design positions specified with respect to the reference detector plane, beams are computed with nine sampling frequencies, $W_B = W_{3dB}$, $W_F = (W_{max}W_{min})^{1/2}$)

HFI beam	W_{max} arcmin	W_{min} arcmin	φ_{SC0} deg	η_{SC0} deg	τ deg	W_B arcmin	W_F arcmin	G_B dBi	G_F dBi	ϵ_F	δF %	δL %	δV %
100-1a	10.4560	8.9481	1.1842	3.5120	13.5124	9.90	9.67	60.33	60.40	1.169	1.9	0.4	2.1
100-1b	10.4505	8.9528	1.1842	3.5120	13.4052	9.88	9.67	60.33	60.40	1.167	1.8	0.4	2.0
100-2a	10.5047	8.9918	0.3829	3.2410	4.4241	10.05	9.72	60.61	60.70	1.168	2.1	0.4	1.3
100-2b	10.5000	8.9943	0.3830	3.2410	3.6527	10.05	9.72	60.61	60.70	1.167	2.1	0.4	1.3
100-3a	10.5147	8.9839	-0.3829	3.2411	-3.9942	10.05	9.72	60.61	60.70	1.170	2.1	0.4	1.3
100-3b	10.4899	9.0024	-0.3829	3.2410	-4.0856	10.05	9.72	60.61	60.70	1.165	2.0	0.4	1.3
100-4a	10.4579	8.9491	-1.1842	3.5120	-13.5110	9.90	9.67	60.33	60.41	1.169	1.9	0.4	2.1
100-4b	10.4525	8.9539	-1.1842	3.5120	-13.4058	9.88	9.67	60.33	60.41	1.167	1.8	0.4	2.0

HFI beam	W_{max} arcmin	W_{min} arcmin	φ_{SC0} deg	η_{SC0} deg	τ deg	W_B arcmin	W_F arcmin	G_B dBi	G_F dBi	ϵ_F	δF %	δL %	δV %
143-1a	7.4323	6.8745	1.3718	6.1966	49.6927	7.30	7.15	63.44	63.51	1.081	2.1	0.9	4.0
143-1b	7.4986	6.8574	1.3717	6.1966	49.0453	7.35	7.17	63.41	63.48	1.094	2.0	1.0	4.2
143-2a	7.1939	6.9619	0.5637	6.2243	61.3503	7.29	7.08	63.54	63.62	1.033	2.2	0.6	3.7
143-2b	7.2439	6.9324	0.5637	6.2243	56.6716	7.32	7.09	63.52	63.60	1.045	2.2	0.5	3.8
143-3a	7.2249	6.9377	-0.5637	6.1992	-61.7208	7.32	7.08	63.53	63.61	1.041	2.2	0.7	3.7
143-3b	7.1967	6.9460	-0.5637	6.1993	-52.9134	7.29	7.07	63.54	63.62	1.036	2.2	0.5	3.8
143-4a	7.5149	6.8715	-1.4418	6.2210	-51.4655	7.33	7.19	63.40	63.47	1.094	2.0	1.2	4.2
143-4b	7.5083	6.8790	-1.4419	6.2211	-47.3673	7.33	7.19	63.40	63.47	1.091	2.0	1.0	4.3
143-5	7.5902	7.1702	1.1443	6.7334	62.8153	7.50	7.38	66.23	66.29	1.059	2.1	0.5	4.5
143-6	7.3981	7.1650	0.2997	6.7608	79.0498	7.41	7.28	66.34	66.41	1.033	2.0	0.5	4.2
143-7	7.3836	7.1576	-0.2997	6.7358	-78.5876	7.41	7.27	66.35	66.42	1.032	2.0	0.5	4.2
143-8	7.6067	7.1833	-1.1443	6.7585	-63.2693	7.51	7.39	66.21	66.27	1.059	2.1	0.5	4.5
217-1	5.0748	4.4924	0.9960	4.0142	12.1172	4.88	4.77	70.03	70.10	1.130	2.0	0.2	1.5
217-2	5.0071	4.5114	0.3149	4.0403	4.3963	4.86	4.75	70.08	70.15	1.110	2.1	0.2	0.5
217-3	5.0086	4.5070	-0.3148	4.0153	-4.3277	4.85	4.75	70.08	70.15	1.111	2.1	0.2	0.5
217-4	5.0725	4.4947	-0.9961	4.0391	-12.3129	4.88	4.77	70.03	70.10	1.129	2.0	0.2	1.5
217-5a	5.0741	4.5330	1.2256	4.5149	18.5837	4.90	4.80	66.96	67.02	1.119	2.2	0.4	2.0
217-5b	5.0718	4.5339	1.2257	4.5149	18.3535	4.90	4.80	66.97	67.03	1.119	2.2	0.4	2.0
217-6a	4.9771	4.5835	0.5435	4.5416	10.9266	4.87	4.78	67.01	67.08	1.086	2.2	0.3	1.2
217-6b	4.9756	4.5841	0.5436	4.5416	10.5525	4.87	4.78	67.01	67.08	1.085	2.2	0.3	1.2
217-7a	4.9781	4.5773	-0.5435	4.5166	-10.4282	4.87	4.77	67.02	67.09	1.088	2.2	0.3	1.2
217-7b	4.9755	4.5798	-0.5435	4.5166	-10.5638	4.88	4.77	67.02	67.09	1.086	2.2	0.2	1.2
217-8a	5.0733	4.5354	-1.2258	4.5399	-18.7074	4.90	4.80	66.97	67.03	1.119	2.2	0.4	2.0
217-8b	5.0716	4.5377	-1.2258	4.5399	-18.8780	4.90	4.80	66.96	67.03	1.118	2.2	0.4	2.1
353-1	5.1917	4.1539	2.0626	5.0155	21.7076	4.66	4.64	70.58	70.60	1.250	2.0	0.1	2.4
353-2	4.9061	4.2351	1.4195	5.0436	21.9361	4.66	4.56	70.74	70.79	1.158	1.6	0.1	1.8
353-3a	4.7513	4.3493	0.8248	5.0204	19.6160	4.66	4.55	67.68	67.74	1.092	1.6	0.7	1.3
353-3b	4.7513	4.3500	0.8248	5.0204	19.5862	4.66	4.55	67.68	67.74	1.092	1.6	0.6	1.3
353-4a	4.6682	4.4435	0.2107	5.0462	8.4538	4.64	4.55	67.67	67.74	1.051	1.6	0.5	1.2
353-4b	4.6681	4.4437	0.2108	5.0462	8.3505	4.64	4.55	67.67	67.74	1.051	1.6	0.4	1.2
353-5a	4.6832	4.4224	-0.3687	5.0211	-12.6675	4.64	4.55	67.68	67.75	1.059	1.6	0.3	1.2
353-5b	4.6822	4.4220	-0.3687	5.0211	-12.6907	4.64	4.55	67.68	67.75	1.059	1.6	0.4	1.1
353-6a	4.7825	4.3264	-0.9650	5.0451	-21.0534	4.65	4.55	67.68	67.75	1.105	1.6	0.5	1.6
353-6b	4.7812	4.3252	-0.9650	5.0451	-21.0458	4.64	4.55	67.68	67.75	1.105	1.6	0.5	1.5
353-7	4.9395	4.2137	-1.5240	5.0181	-21.4681	4.64	4.56	70.73	70.78	1.172	1.7	0.1	1.9
353-8	5.1953	4.1554	-2.0628	5.0406	-22.1009	4.69	4.65	70.58	70.61	1.250	2.0	0.1	2.4
545-1	4.4859	3.7289	2.0686	5.5336	35.5850	4.77	4.09	75.74	76.33	1.203	25.8	1.9	7.0
545-2	3.8050	3.3962	1.4230	5.5632	41.3291	4.40	3.59	76.84	77.47	1.120	40.3	3.1	7.1
545-3	3.8636	3.4156	-1.5279	5.5376	-40.2154	4.40	3.63	76.75	77.38	1.131	38.6	2.9	7.3
545-4	4.5011	3.7395	-2.0688	5.5585	-35.9540	4.82	4.10	75.71	76.30	1.204	25.6	1.9	7.0
857-1	3.9595	3.6561	0.8440	5.5381	37.0723	4.93	3.80	79.77	80.46	1.083	36.6	10.0	2.7
857-2	3.8445	3.7628	0.2288	5.5641	37.9611	4.95	3.80	79.73	80.47	1.022	37.3	10.3	2.2
857-3	3.8642	3.7386	-0.3519	5.5390	-37.0791	4.91	3.80	79.75	80.48	1.034	37.3	10.3	2.1
857-4	3.9924	3.6410	-0.9669	5.5628	-37.4161	4.93	3.81	79.73	80.43	1.097	36.7	9.8	3.2